Journal of Petroleum Science and Engineering 208 (2022) 109655

Contents lists available at ScienceDirect

Journal of Petroleum Science and Engineering

journal homepage: www.elsevier.com/locate/petrol

Energy transport of wavy non-homogeneous hybrid nanofluid cavity partially filled with porous LTNE layer

Ammar I. Alsabery [a,b], Ahmad Hajjar [c], Zehba A.S. Raizah [d], Mohammad Ghalambaz [e,f], Ishak Hashim [b,*], Ali J. Chamkha [g,h]

[a] Refrigeration & Air-conditioning Technical Engineering Department, College of Technical Engineering, The Islamic University, Najaf, Iraq
[b] Department of Mathematical Sciences, Faculty of Science & Technology, Universiti Kebangsaan Malaysia, 43600 UKM Bangi, Selangor, Malaysia
[c] ECAM Lyon, LabECAM, University of Lyon, Lyon, France
[d] Department of Mathematics, College of Science, Abha, King Khalid University, Saudi Arabia
[e] Metamaterials for Mechanical, Biomechanical and Multiphysical, Applications Research Group, Ton Duc Thang University, Ho Chi Minh City, Viet Nam
[f] Faculty of Applied Sciences, Ton Duc Thang University, Ho Chi Minh City, Viet Nam
[g] Faculty of Engineering, Kuwait College of Science and Technology, Doha District 35004, Kuwait
[h] Center of Excellence in Desalination Technology, King Abdulaziz University, P.O. Box 80200, Jeddah 21589, Saudi Arabia

ARTICLE INFO

Keywords:
Natural convection
Hybrid nanofluid-porous cavity
Amplitude
Darcy–Forchheimer model
Local thermal non-equilibrium (LTNE)

ABSTRACT

The two-phase flow and heat transfer of a Cu–Al_2O_3 water hybrid nanofluid in a wavy enclosure partially filled with a porous medium is investigated. The concentration gradient of the composite nanoparticles is modeled considering the thermophoresis and Brownian motion nanoscale forces. The porous medium is also modeled using the local thermal non-equilibrium model. The governing equations are converted into a non-dimensional form and then solved using the finite element technique. The impact of the Darcy number, convection interface, and the wave amplitude on the concentration distribution of nanoparticle flow and heat transfer is addressed. The outcomes show that the convective heat transfer in the liquid and solid phases could be increased by 4.5 and 2.7 folds by increasing the Darcy number from 10^{-5} to 10^{-2}. The growth of the concentration of the nanoparticles from 0 to 0.04 improves the liquid Nusselt number by 17%. The hybrid nanofluid shows a better heat transfer enhancement compared to simple nanofluids.

1. Introduction

The transfers of heat energy become a necessary task for world industry. The improvement of heat transfer in an industrial process can minimize process time, saving energy, thermal rate rising and keeping the life of the equipment work. There are comprehensive methods of enhancement heat transfer in mechanical systems. Some of them are the utilization of the porous medium. However, there are wide heat transfer applications in porous media, as mentioned in Nield et al. (2006), Rashed et al. (2021). It is useful in the recovery and storage of energy, the building's insulation, reservoirs of geothermal, the storage of grain and coal, chemical reactor engineering, etc. The porous layer inside a cavity partly saturated by a porous layer may be oriented either horizontally (Filahi et al., 2021; Celli et al., 2020; Mutschler and Mojtabi, 2020) or vertically (Miroshnichenko et al., 2018; Selimefendigil and Öztop, 2020). Researchers have presented the famous models of non-Darcy models to analyze the flow through the porous media: The Darcy–Brinkman model and the Forchheimer–Brinkman-extended Darcy model.

For example, to use the Forchheimer–Darcy–Brinkman model to study nanofluids' convection, one can refer to the studies (Sivasankaran et al., 2011; Ambreen et al., 2020; Das et al., 2016; Khoei et al., 2020; Nayak et al., 2020; Haider et al., 2021). Hussain et al. (2020) reported on the heat transfer in an open trapezoidal cavity holding a porous layer using the Darcy–Forchheimer model. Aly and Raizah (2020) simulated the natural convection inside a wavy cavity that is filled by a partly-layered non-Darcy porous medium in the presence of solid particles. The natural convection in a complex cavity saturated by Fe_3O_4-water nanofluid and porous media was presented by Molana et al. (2020). To explain the heat properties inside porous media numerically, there are two approaches. First, the local thermal equilibrium (LTE) approach, which adopted in the studies of Nguyen et al. (2015), Chen et al. (2016), Sheremet et al. (2017a), Ghasemi and Siavashi (2017) and Almuhtady et al. (2021), and the other is named the local thermal non-equilibrium (LTNE) approach, which was applied in Chen et al. (2018), Wang et al. (2019), Ghalambaz et al. (2019), Mikhailenko and Sheremet (2020), Mehryan et al. (2020) and Zhang et al. (2021).

* Corresponding author.
E-mail addresses: mohammad.ghalambaz@tdtu.edu.vn (M. Ghalambaz), ishak_h@ukm.edu.my (I. Hashim).

https://doi.org/10.1016/j.petrol.2021.109655
Received 15 July 2021; Received in revised form 21 September 2021; Accepted 10 October 2021
Available online 16 October 2021

Nomenclature

A	Amplitude
D	Dimensionless thickness of the nanofluid layer, $D = d/L$
Da	Darcy number
D_B	Brownian diffusion coefficient
D_{B0}	Reference Brownian diffusion coefficient
d_f	Diameter of the base fluid molecule
d_p	Diameter of the nanoparticle
D_T	Thermophoretic diffusivity coefficient
D_{T0}	Reference thermophoretic diffusion coefficient
C_p	Specific heat capacity
g	Gravitational acceleration
H	Inter-phase heat transfer coefficient
k	Thermal conductivity
K	Permeability of the porous medium
L	Width and height of the square cavity
Le	Lewis number
N	Number of undulations
N_{BT}	Ratio of Brownian to thermophoretic diffusivity
$\overline{Nu}$	Average Nusselt number
Pr	Prandtl number
Ra	Rayleigh number
Re_B	Brownian motion Reynolds number
T	Temperature
T_{fr}	Freezing point of the base fluid (273.15 K)
$\mathbf{v}$, $\mathbf{V}$	Velocity and dimensionless velocity vector
u_B	Brownian velocity of the nanoparticle
x, y&X, Y	Space coordinates & dimensionless space coordinates

Greek symbols

α	Thermal diffusivity
β	Thermal expansion coefficient
γ	Modified conductivity ratio
ε	Porosity of the medium
δ	Normalized temperature parameter
θ	Dimensionless temperature
μ	Dynamic viscosity
ν	Kinematic viscosity
ρ	Density
φ	Solid volume fraction
φ^*	Normalized solid volume fraction
ϕ	Average solid volume fraction

subscript

b	Bottom
c	Cold
f	Base fluid
h	Hot
m	Porous layer (porous media)
nf	Nanofluid phase
p	Solid nanoparticles
s	Solid phase

The LTE model depends on only one energy equation to describe the heat transfer because this model takes the solid matrix and the saturated fluid together in local thermodynamic equilibrium. While in the LTNE model, it is necessary to take two energy equations to control the up-growth of temperature for the fluid and solid phases. The LTE and LTNE models' advancement is summarized in the paper of Baytas and Pop (2002). Alomar et al. (2020) investigated the convective heat transfer inside a square porous cavity containing two perpendicular plates using a non-Darcian flow and the Local Thermal Non-Equilibrium (LTNE) assumptions. Under the LTNE approach, Wang et al. (2021) investigated free convection in a porous cavity with an internal circular cylinder. They indicated that the solid heat transfer rate increased as the LTNE parameters increased.

Several experimental and numerical investigations on nanofluid flow and heat transfer through porous media inside a cavity with a wavy surface were presented. A famous technique used for enhancement of heat transfer inside cavities is applying complex geometry shapes like wavy shapes because they have more area than the regular shapes (Misirlioglu et al., 2005; Revnic et al., 2020). The wavy shape through a square cavity's left wall filled with a heat-generating porous medium was analyzed by Ahmed and Rashed (2019). They observed that both the undulation number and the wavy contraction ratio improve the heat transfer rate. Natural convection within a tilted curved open porous enclosure filled by nanofluids was investigated by Bondareva et al. (2016). Oğlakkaya and Bozkaya (2018) investigated the unsteady mixed convection numerically into a lid-driven cavity including sinusoidal curved surface. Alsabery et al. (2018) explained the convective flow and heat transfer inside a base heated curved porous enclosure. The simulation of a nanofluid's natural convection into a wavy enclosure including partly-layered non-Darcy porous medium was studied by Aly and Raizah (2020) and Elshehabey et al. (2020). Under the impact of a uniform vertical magnetic field, Parveen and Mahapatra (2019) provided a numerical investigation of steady double-diffusive free convection from water-based nanofluid inside a curved cavity with an interior heater. More examples of applied wavy walls of the cavities can be found in the studies (Shenoy et al., 2016; Alsabery et al., 2019a; Ashorynejad and Shahriari, 2018; Cho, 2020; Rashed et al., 2020; Sadeghi et al., 2021). They all determined that the heat and mass transfer was affected by the number of the wave wall and its amplitude.

For many past years, researchers and engineers in the field of fluids have introduced their work using nanofluids due to their properties that make them distinct and more effective than the traditional fluids. To analyze the nanofluids numerically, different methods for classifying them within two groups: Single-phase and two-phase approaches. Moreover, the two-phase approach has various methods, namely the Eulerian Mixture model (EMM) (Li et al., 2019; Bozorg and Siavashi, 2019), Eulerian–Lagrangian model (Borah and Pati, 2021), the volume of fluid (VOF) (Chen et al., 2016), Eulerian–Eulerian model (Mehryan et al., 2020), Buongiorno model (Ahmed and Rashed, 2019; Bondareva et al., 2016; Oğlakkaya and Bozkaya, 2018; Alsabery et al., 2018; Elshehabey et al., 2020; Parveen and Mahapatra, 2019; Shenoy et al., 2016; Alsabery et al., 2019a; Ashorynejad and Shahriari, 2018; Cho, 2020; Rashed et al., 2020; Sadeghi et al., 2021; Li et al., 2019; Bozorg and Siavashi, 2019; Borah and Pati, 2021; Sheremet et al., 2017b; Alsabery et al., 2019b, 2020), and the double-diffusive model (Raizah and Aly, 2021). The two-phase nanofluid model has the ability to enhance the heat transfer and energy efficiency in thermal systems, so it is applied in many industrial fields, such as power electronics, transportation, microelectronics, heat pipes, nuclear engineering, air-conditioning, refrigeration, and heat pump systems.

According to the above literature review and to the best of the authors' knowledge, no investigation was reported on convection heat transfer inside a partially filled porous wavy cavity with the application of the local thermal non-equilibrium condition. Therefore, this fundamental study primary examines the influence of non-homogeneous hybrid nanofluid and the local thermal non-equilibrium method on natural convection into a wavy cavity partly filled with a porous layer. This investigation can enhance the cooling of electric, electronic and nuclear designs and control the fluid movement and heat transfer of

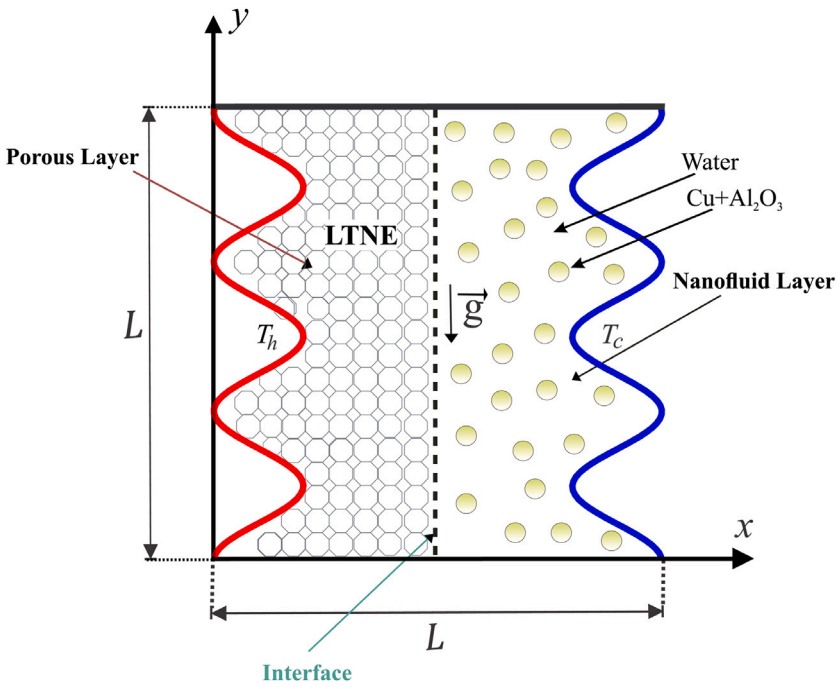

Fig. 1. Physical model of the wavy-walled cavity together with the coordinate system.

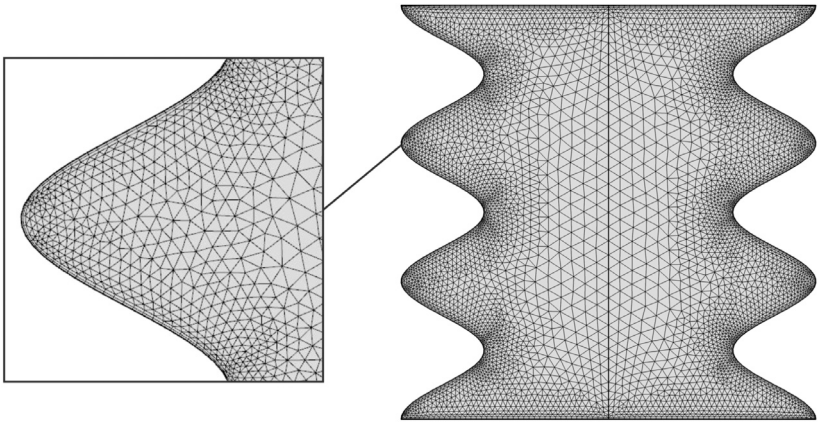

Fig. 2. FEM grid-points distribution for the grid size of 10222 elements.

the solar thermal processes, thermal domain and porous media applications. Also, such a study will be significant in processing composite materials, nuclear reactor maintenance, flows in microchannels and convection in stellar atmospheres.

2. Mathematical formulation

Two-dimensional steady-state natural convection in a wavy cavity partly filled with a porous layer with length L is represented by Fig. 1. The examined cavity is divided into two layers (segments). The first layer remains loaded with a porous material that is saturated by a hybrid nanofluid, and the second layer is filled with a hybrid nanofluid. The wavy (vertical left) surface is kept at a fixed hot temperature of T_h, while the vertical right wavy surface remains fixed at a constant cold temperature T_c. In contrast, the top and bottom horizontal surfaces remain preserved adiabatic. The edges regarding the domain are considered impermeable except the interface surface which remains permeable; and the liquid inside the examined cavity is a water-based hybrid nanofluid holding Cu-Al_2O_3 nanoparticles. The Forchheimer–Brinkman-extended Darcy model along with the Boussinesq approximation, are relevant. Furthermore, the hybrid nanofluid phase's convection and the solid matrix are in a local thermodynamic non-equilibrium state. The type of porous media is considered as glass balls. Acknowledging the specified theories, the continuity, momentum and energy equations for laminar Newtonian flow would be addressed as follows:

For the hybrid nanofluid layer:

$$\nabla \cdot \mathbf{v}_{hnf} = 0, \tag{1}$$

$$\rho_{hnf}\mathbf{v}_{hnf} \cdot \nabla \mathbf{v}_{hnf} = -\nabla p + \nabla \cdot (\mu_{hnf} \nabla \mathbf{v}_{hnf}) + (\rho\beta)_{hnf}(T - T_c)\vec{g}, \tag{2}$$

$$(\rho C_p)_{hnf}\mathbf{v}_{hnf} \cdot \nabla T_{hnf} = \nabla \cdot (k_{hnf} \nabla T_{hnf}) - C_{p,p}\mathbf{J}_p \cdot \nabla T_{hnf}, \tag{3}$$

$$\mathbf{v}_{hnf} \cdot \nabla \varphi = -\frac{1}{\rho_p} \nabla \cdot \mathbf{J}_p. \tag{4}$$

For the porous layer:

$$\nabla \cdot \mathbf{v}_m = 0, \tag{5}$$

$$\frac{\rho_{hnf}}{\varepsilon^2}\left(\mathbf{v}_m \cdot \nabla \mathbf{v}_m\right) = -\nabla p + \nabla \cdot \left(\frac{\mu_{hnf}}{\varepsilon} \nabla \mathbf{v}_m\right) - \left(\frac{\mu_{hnf}}{K}\mathbf{v}_m - F\frac{\rho_{hnf}\mathbf{v}_m |\mathbf{u}|}{\sqrt{K}}\right) + (\rho\beta)_{hnf}(T - T_c)\vec{g}, \tag{6}$$

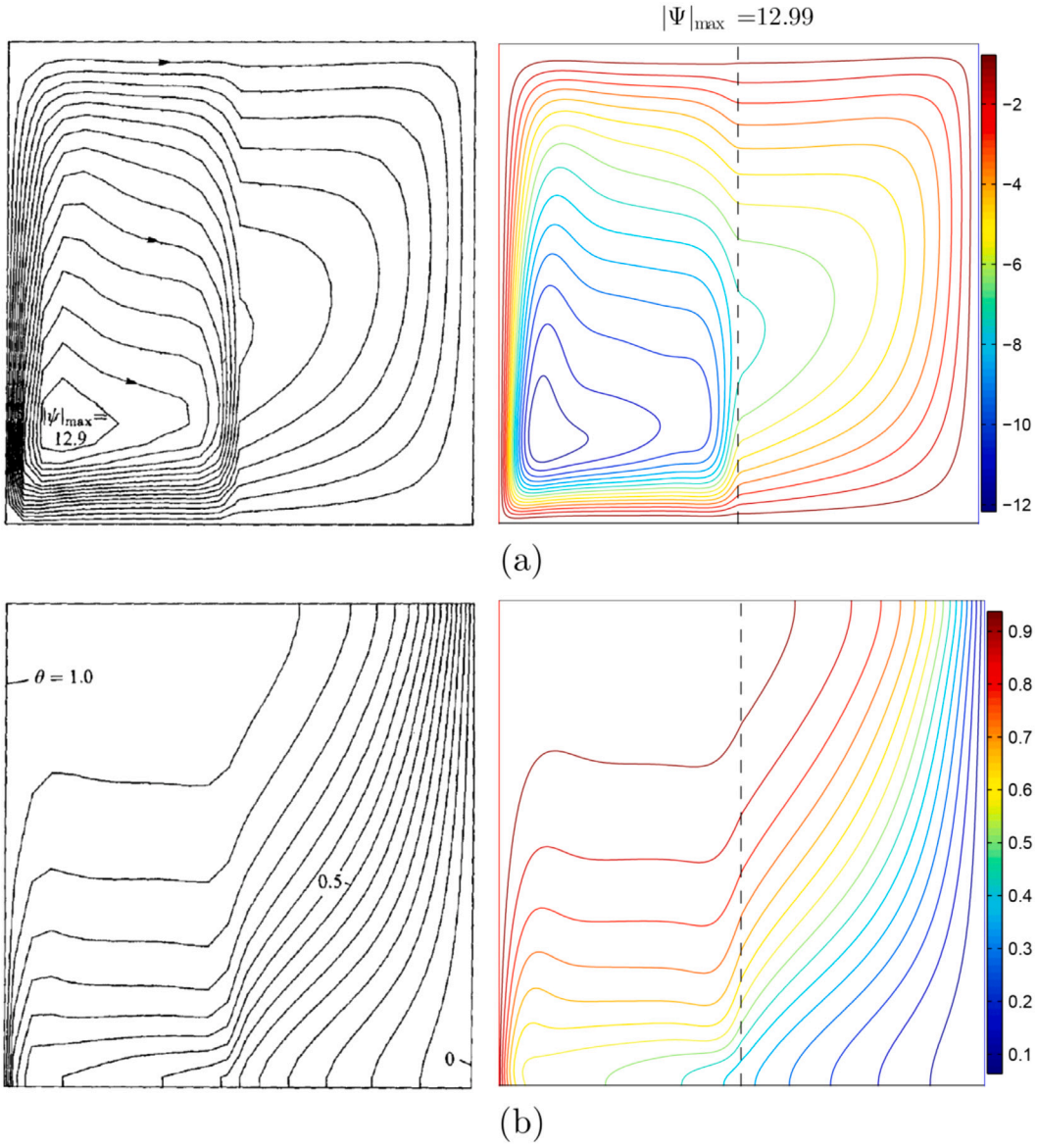

Fig. 3. (a) streamlines of Beckermann et al. (1988) (left) and present study (right); (b) isotherms for $Ra = 3.70 \times 10^6$, $Da = 1.370 \times 10^{-5}$, $\varepsilon = 0.9$, $D = 0.5$ $N = 0$, $\frac{k_{eff}}{k_f} = 1.362$ and Pr = 6.44.

$$(\rho C_p)_{hnf}\left(\mathbf{v}_m \cdot \nabla T_m\right) = \nabla \cdot \left(\varepsilon k_{hnf} \nabla T_m\right) - \varepsilon C_{p,p} J_p \cdot \nabla T_m + h\left(T_s - T_m\right), \quad (7)$$

$$0 = (1-\varepsilon) k_s \left(\nabla T_s\right) + h\left(T_m - T_s\right), \quad (8)$$

$$\frac{1}{\varepsilon}\left(\mathbf{v}_m \cdot \nabla \varphi\right) = -\frac{1}{\rho_p} \nabla \cdot J_p, \quad (9)$$

where the subscripts hnf, m and s stand for the hybrid nanofluid layer, porous layer (nanofluid phase) and porous layer (solid phase), respectively. $|\mathbf{u}| = \sqrt{u^2 + v^2}$ is the Darcy velocity, $\vec{g}$ is the acceleration due to gravity and ε is the porosity of the medium.

K is shown the permeability of the porous medium which is defined as follows:

$$K = \frac{\varepsilon^3 d_m^2}{150(1-\varepsilon)^2}. \quad (10)$$

Based on the two-phase approach, the nanoparticles mass flux (J_p) is formulated as:

$$J_p = J_{p,B} + J_{p,T}, \quad (11)$$

$$J_{p,B} = -\rho_p D_B \nabla \varphi, \quad D_B = \frac{k_b T}{3\pi \mu_f d_p}, \quad (12)$$

$$J_{p,T} = -\rho_p D_T \frac{\nabla T}{T}, \quad D_T = 0.26 \frac{k_f}{2k_f + k_p} \frac{\mu_f}{\rho_f T} \varphi. \quad (13)$$

Here d_m represents the medium particle dimension regarding the porous bed.

The hybrid nanofluids adequate physical features remain performed into the following system:

The hybrid nanofluid heat capacitance $(\rho C_p)_{hnf}$ is provided as:

$$\left(\rho C_p\right)_{hnf} = \varphi_{Cu}\left(\rho C_p\right)_{Cu} + \varphi_{Al_2O_3}\left(\rho C_p\right)_{Al_2O_3} + \left(1 - \varphi_{Cu} - \varphi_{Al_2O_3}\right)\left(\rho C_p\right)_f. \quad (14)$$

The hybrid nanofluid density ρ_{hnf} is present as:

$$\rho_{hnf} = \varphi_{Cu}\rho_{Cu} + \varphi_{Al_2O_3}\rho_{Al_2O_3} + \left(1 - \varphi_{Cu} - \varphi_{Al_2O_3}\right)\rho_f. \quad (15)$$

The hybrid nanofluid buoyancy coefficient $(\rho\beta)_{hnf}$ is defined by:

$$(\rho\beta)_{hnf} = \varphi_{Cu}(\rho\beta)_{Cu} + \varphi_{Al_2O_3}(\rho\beta)_{Al_2O_3} + \left(1 - \varphi_{Cu} - \varphi_{Al_2O_3}\right)(\rho\beta)_f. \quad (16)$$

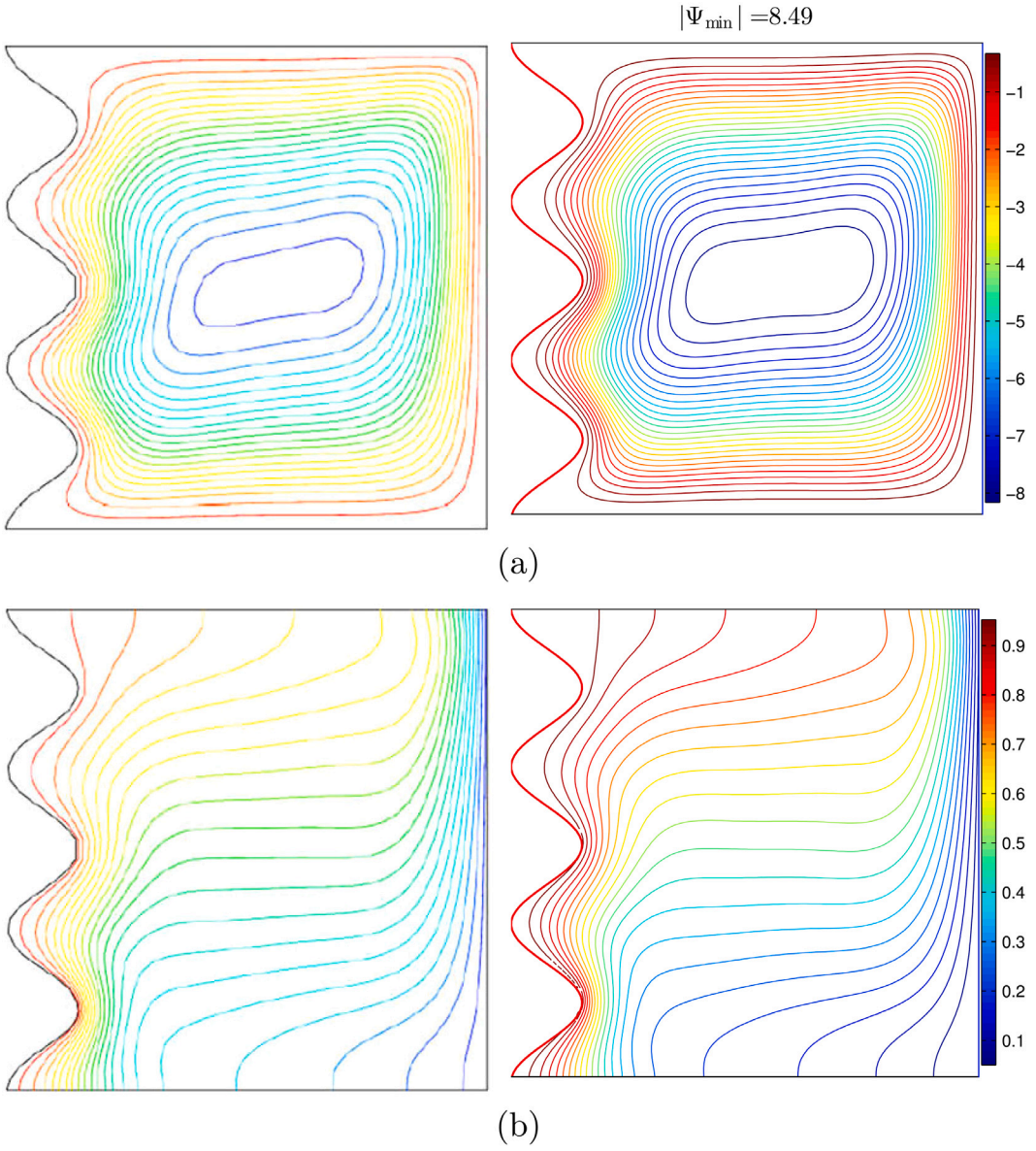

Fig. 4. Streamlines of (left) Khanafer et al. (2009) and (right) current work; (b) isotherms of (left) Khanafer et al. (2009) and (right) current work for $Ra = 10^5$, $Da = 10^{-2}$, $\varepsilon = 0.9$, $N = 3$ and Pr = 1.

The dynamic viscosity ratio concerning nanofluids is obtained by Corcione (2011):

$$\frac{\mu_{nf}}{\mu_f} = \frac{1}{1 - 34.87\left(\frac{d_p}{d_f}\right)^{-0.3}\varphi^{1.03}}. \tag{17}$$

and the thermal conductivity ratio concerning nanofluids is estimated through the Corcione et al. model (Corcione, 2011) as:

$$\frac{k_{nf}}{k_f} = 1 + 4.4\mathrm{Re}_B^{0.4}\mathrm{Pr}^{0.66}\left(\frac{T}{T_{fr}}\right)^{10}\left(\frac{k_p}{k_f}\right)^{0.03}\varphi^{0.66}, \tag{18}$$

Using the above discussed models, we perform innovative forms associated with the dynamic viscosity ratio and thermal conductivity ratio of water-Cu-Al_2O_3 hybrid nanofluid toward 33 and 29 nm particles by the following:

$$\frac{\mu_{hnf}}{\mu_f} = \frac{1}{1 - 34.87\,(d_f)^{0.3}\left[(d_{\mathrm{Cu}})^{-0.3}(\varphi_{\mathrm{Cu}})^{1.03} + \left(d_{\mathrm{Al_2O_3}}\right)^{-0.3}\left(\varphi_{\mathrm{Al_2O_3}}\right)^{1.03}\right]}, \tag{19}$$

$$\frac{k_{hnf}}{k_f} = 1 + 4.4\mathrm{Re}_B^{0.4}\mathrm{Pr}^{0.66}\left(\frac{T}{T_{fr}}\right)^{10}(k_f)^{-0.03} \times \left[(k_{\mathrm{Cu}})^{0.03}(\varphi_{\mathrm{Cu}})^{0.66} + \left(k_{\mathrm{Al_2O_3}}\right)^{0.03}\left(\varphi_{\mathrm{Al_2O_3}}\right)^{0.66}\right], \tag{20}$$

where Re_B of the hybrid nanofluid is defined as:

$$\mathrm{Re}_B = \frac{\rho_f u_B\left(d_{\mathrm{Cu}} + d_{\mathrm{Al_2O_3}}\right)}{\mu_f}, \quad u_B = \frac{2k_bT}{\pi\mu_f\left(d_{\mathrm{Cu}} + d_{\mathrm{Al_2O_3}}\right)^2}. \tag{21}$$

The molecular diameter of water (d_f) is computed by Corcione (2011):

$$d_f = 0.1\left[\frac{6M}{N^*\pi\rho_f}\right]^{\frac{1}{3}}. \tag{22}$$

The following non-dimensional variables are now proposed as:

$$\mathbf{V}_{(hnf,m)} = \frac{\mathbf{v}_{(hnf,m)}L}{\nu_f}, \quad P = \frac{pL^2}{\rho_{hnf}\nu_f^2}, \quad \varphi^* = \frac{\varphi}{\phi}, \quad D_B^* = \frac{D_B}{D_{B0}}, \quad D_T^* = \frac{D_T}{D_{T0}},$$

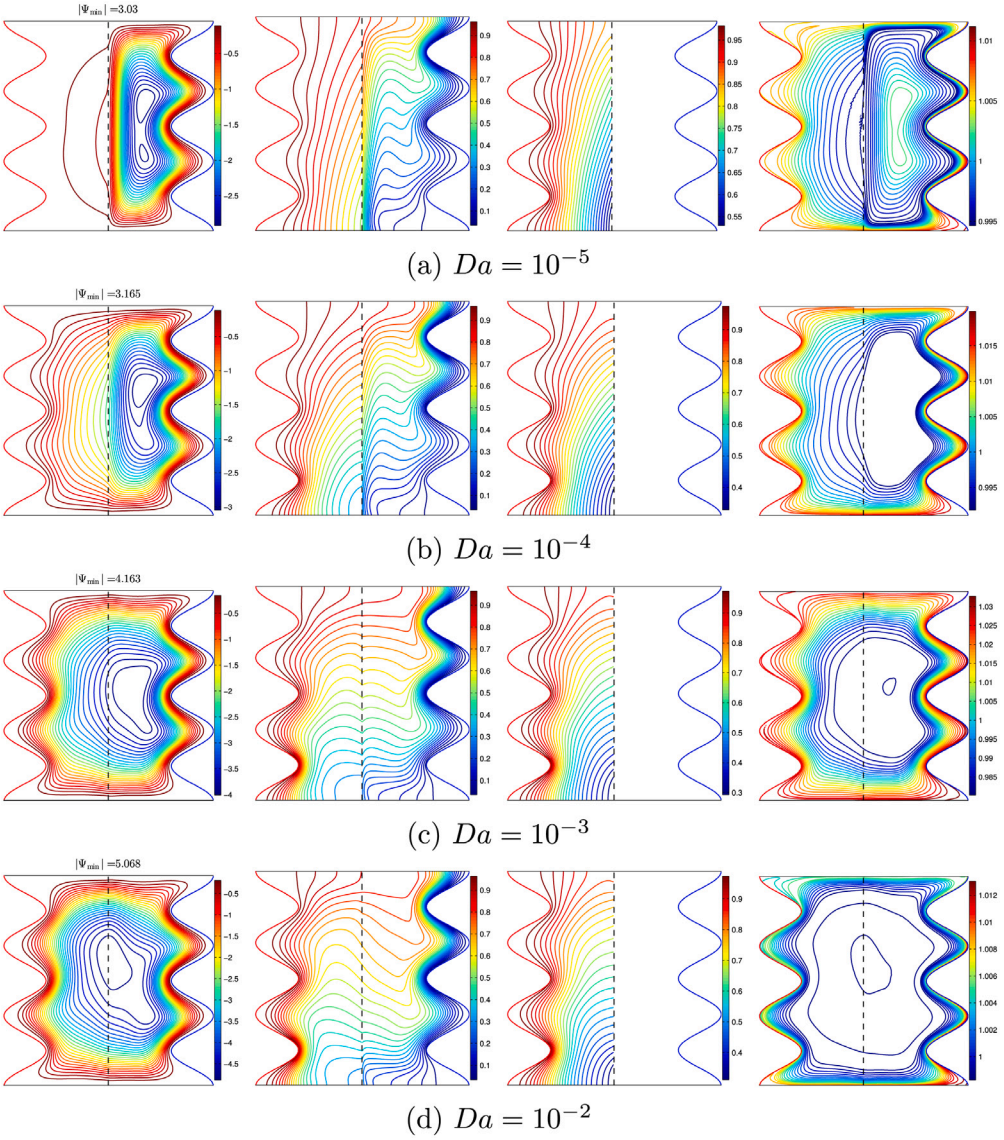

Fig. 5. Streamlines, isotherms of nanofluid phase, isotherms of solid phase and nanoparticle distribution with various Darcy numbers (Da); hybrid nanofluid, $\phi = 0.02$, $\gamma = 10$, $A = 0.1$ and $\varepsilon = 0.5$.

$$\delta = \frac{T_c}{T_h - T_c},\ \theta_{(hnf,m)} = \frac{T_{(hnf,m)} - T_c}{T_h - T_c},$$
$$\theta_s = \frac{T_s - T_c}{T_h - T_c},\ D = \frac{d}{L},\ C_F = \frac{1.75}{\sqrt{150}}. \tag{23}$$

This then yields the following dimensionless governing equations:

In the hybrid nanofluid layer:

$$\nabla \cdot \mathbf{V}_{hnf} = 0, \tag{24}$$

$$\mathbf{V}_{hnf} \cdot \nabla \mathbf{V}_{hnf} = -\nabla P + \frac{\rho_f}{\rho_{hnf}} \frac{\mu_{hnf}}{\mu_f} \nabla^2 \mathbf{V}_{hnf} + \frac{(\rho\beta)_{hnf}}{\rho_{hnf}\beta_f} \frac{1}{\mathrm{Pr}} Ra\theta, \tag{25}$$

$$\mathbf{V}_{hnf} \cdot \nabla \theta_{hnf} = \frac{(\rho C_p)_f}{(\rho C_p)_{hnf}} \frac{k_{hnf}}{k_f} \frac{1}{\mathrm{Pr}} \nabla^2 \theta + \frac{(\rho C_p)_f}{(\rho C_p)_{hnf}} \frac{D_B^*}{\mathrm{Pr} \cdot Le} \nabla \varphi^* \cdot \nabla \theta_{hnf} + \frac{(\rho C_p)_f}{(\rho C_p)_{hnf}} \frac{D_T^*}{\mathrm{Pr} \cdot Le \cdot N_{BT}} \frac{\nabla \theta_{hnf} \cdot \nabla \theta_{hnf}}{1 + \delta\theta_{hnf}}, \tag{26}$$

$$\mathbf{V} \cdot \nabla \varphi^* = \frac{D_B^*}{Sc} \nabla^2 \varphi^* + \frac{D_T^*}{Sc \cdot N_{BT}} \cdot \frac{\nabla^2 \theta_{hnf}}{1 + \delta\theta_{hnf}}. \tag{27}$$

In the porous layer:

$$\nabla \cdot \mathbf{V}_m = 0, \tag{28}$$

$$\frac{1}{\varepsilon^2} \left(\mathbf{V}_m \cdot \nabla \mathbf{V}_m \right) = -\nabla P + \frac{\rho_f}{\rho_{hnf}} \frac{\mu_{hnf}}{\mu_f} \frac{\nabla^2 \mathbf{V}_m}{\varepsilon} - \frac{\rho_f}{\rho_{hnf}} \frac{\mu_{hnf}}{\mu_f} \frac{\mathbf{V}_m}{Da} - \frac{C_F \sqrt{U^2 + V^2}}{\sqrt{Da}} \frac{\mathbf{V}_m}{\varepsilon^{3/2}} + \frac{(\rho\beta)_{hnf}}{\rho_{hnf}\beta_f} \frac{Ra}{\mathrm{Pr}} \theta_m, \tag{29}$$

$$\mathbf{V}_m \cdot \nabla \theta_m = \frac{(\rho C_p)_f}{(\rho C_p)_{\mathrm{eff}}} \frac{k_{\mathrm{eff}}}{k_f} \frac{1}{\mathrm{Pr}} \nabla^2 \theta_m + \frac{(\rho C_p)_f}{(\rho C_p)_{\mathrm{eff}}} \frac{\varepsilon D_B^*}{\mathrm{Pr} \cdot Le} \nabla \varphi^* \cdot \nabla \theta_m + \frac{(\rho C_p)_f}{(\rho C_p)_{\mathrm{eff}}} \frac{\varepsilon D_T^*}{\mathrm{Pr} \cdot Le \cdot N_{BT}} \frac{\nabla \theta \cdot \nabla \theta_m}{1 + \delta\theta_m} + \frac{(\rho C_p)_f}{(\rho C_p)_{hnf}} H\left(\theta_s - \theta_m\right), \tag{30}$$

$$0 = \theta_s + \frac{\partial^2 \theta_s}{\partial Y^2} + \gamma H\left(\theta_m - \theta_s\right), \tag{31}$$

$$\frac{\partial}{\partial \tau} + \frac{1}{\varepsilon} \left(\mathbf{V} \cdot \nabla \varphi^* \right) = \frac{D_B^*}{Sc} \nabla^2 \varphi^* + \frac{D_T^*}{Sc \cdot N_{BT}} \cdot \frac{\nabla^2 \theta}{1 + \delta\theta}. \tag{32}$$

The dimensionless boundary conditions of Eqs. (24)–(32) are:

On the adiabatic top horizontal surface:

$$U = V = 0,\ \frac{\partial \varphi^*}{\partial n} = 0,\ \frac{\partial \theta_{(hnf,m,s)}}{\partial n} = 0, \tag{33}$$

On the left hot wavy surface: $1 - A(1 - \cos(2N\pi X)),\ 0 \le Y \le 1$

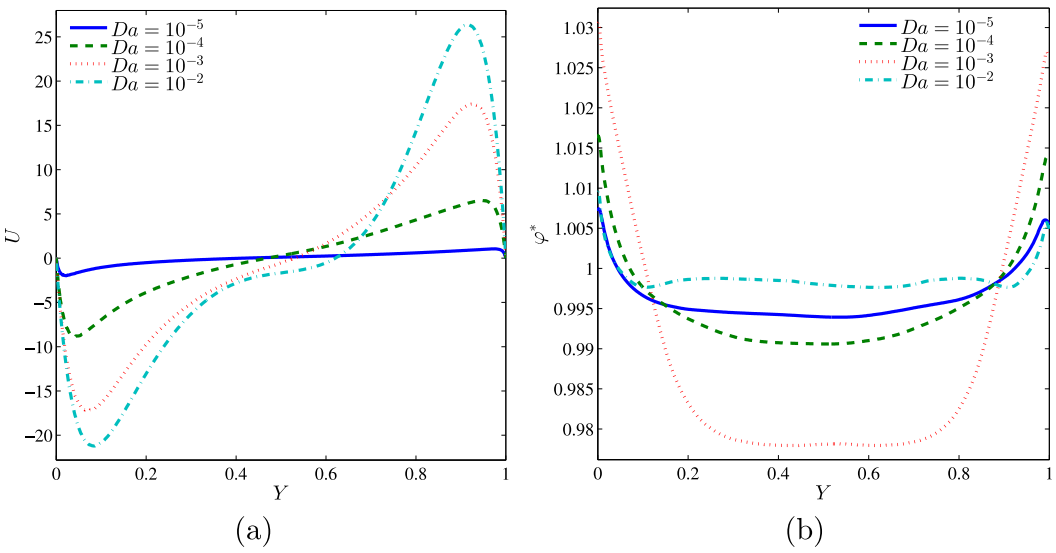

Fig. 6. Local velocity (a) and local normalized solid volume fraction (b) with the vertical line (interface) (Y) for $X = 0.5$ for different Da; hybrid nanofluid, $\phi = 0.02$, $\gamma = 10$, $A = 0.1$ and $\varepsilon = 0.5$.

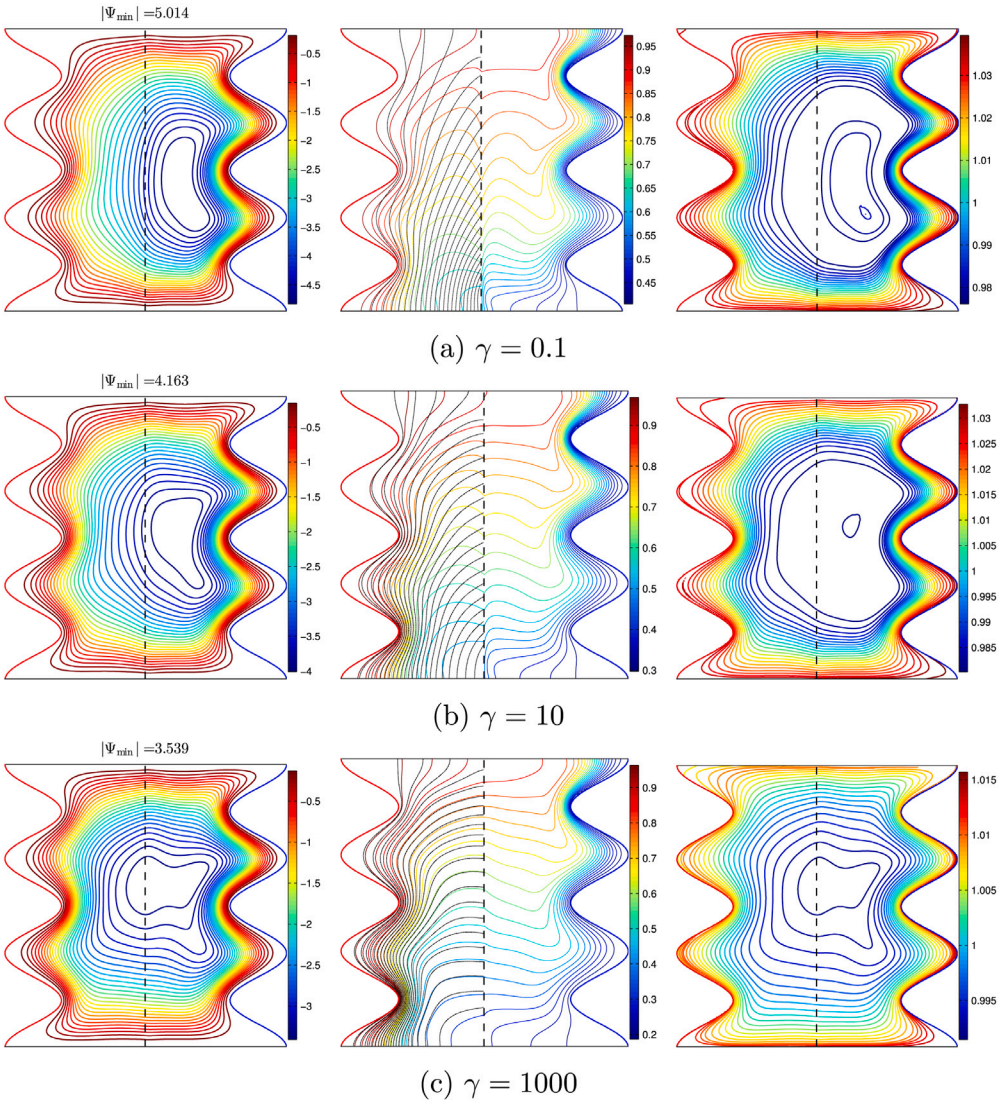

Fig. 7. Streamlines (left), isotherms (solid lines for nanofluid phase and dashed lines for solid phase) (middle), and nanoparticle distribution (right) with various modified conductivity ratios (γ); hybrid nanofluid, $Da = 10^{-3}$, $\phi = 0.02$, $A = 0.1$ and $\varepsilon = 0.5$.

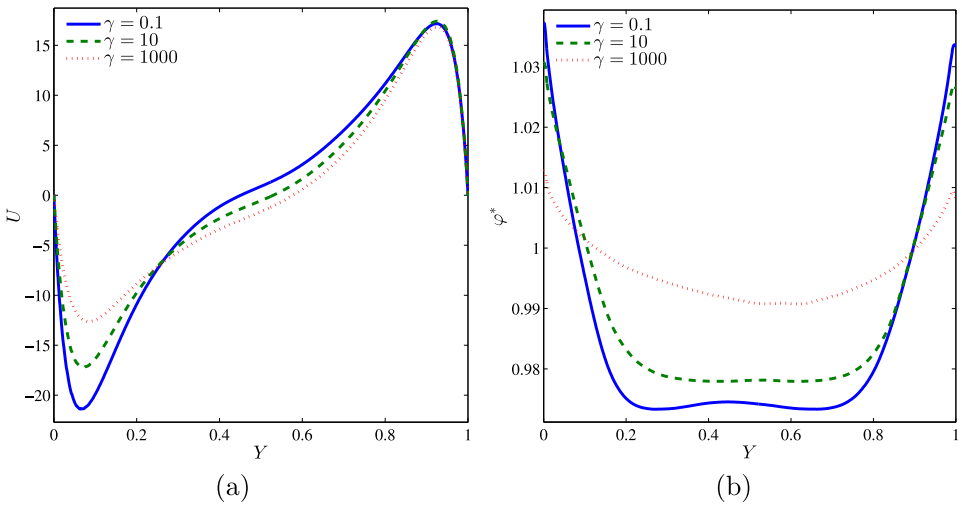

Fig. 8. Local velocity (a) and local normalized solid volume fraction (b) with the vertical line (interface) (Y) for $X = 0.5$ for different γ; hybrid nanofluid, $Da = 10^{-3}$, $\phi = 0.02$, $A = 0.1$ and $\varepsilon = 0.5$.

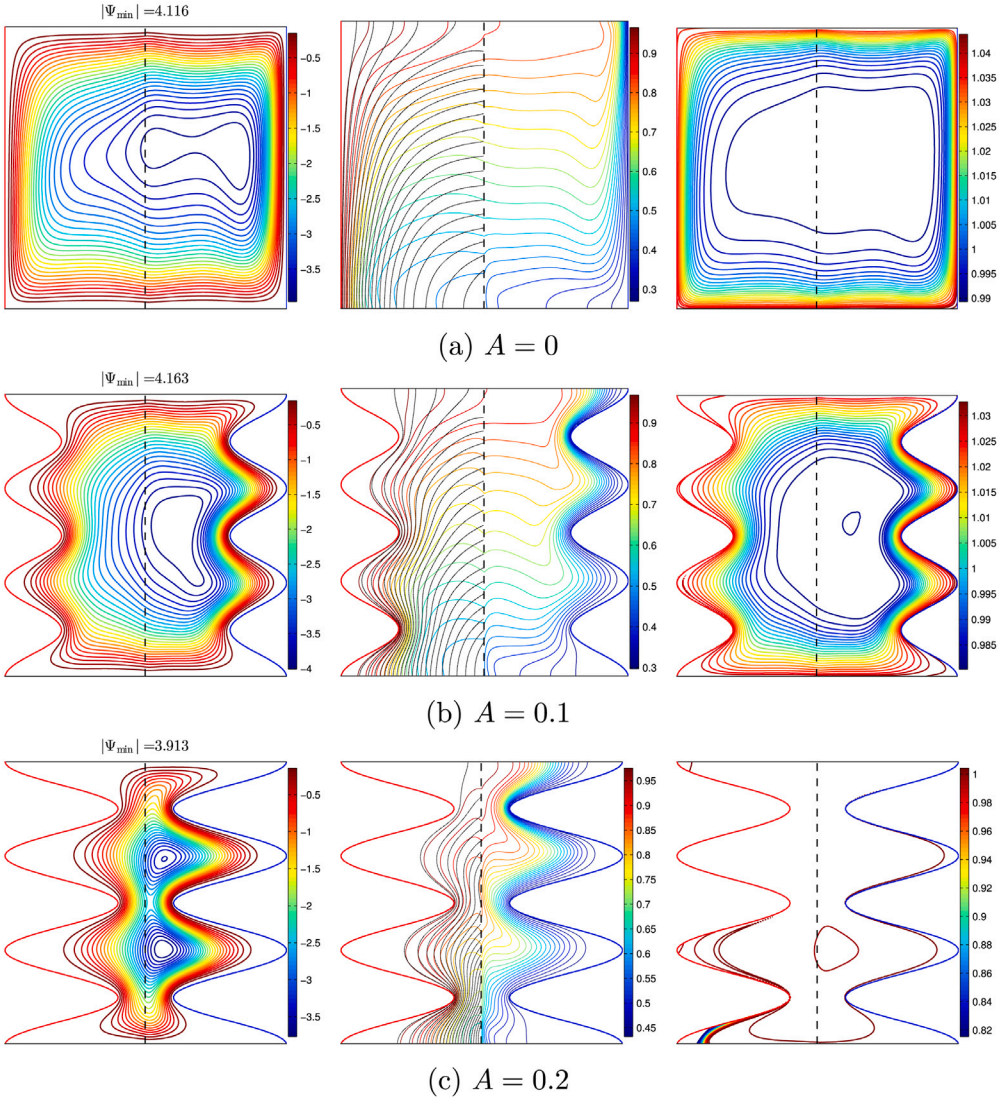

Fig. 9. Streamlines (left), isotherms (solid lines for nanofluid phase and dashed lines for solid phase) (middle), and nanoparticle distribution (right) with various amplitude (A); hybrid nanofluid, $Da = 10^{-3}$, $\phi = 0.02$, $\gamma = 10$ and $\varepsilon = 0.5$.

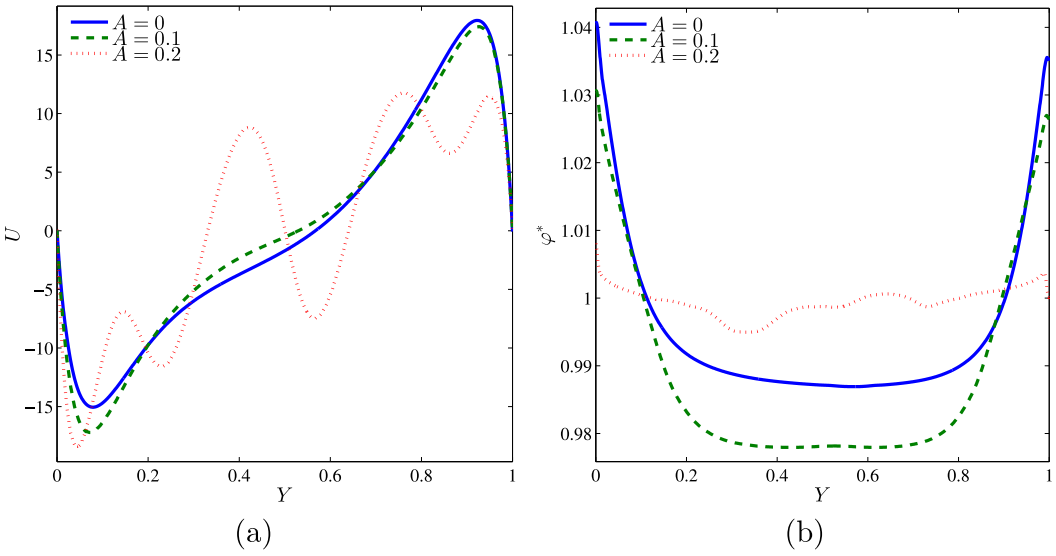

Fig. 10. Local velocity (a) and local normalized solid volume fraction (b) with the vertical line (interface) (Y) for $X = 0.5$ for different A; hybrid nanofluid, $Da = 10^{-3}$, $\phi = 0.02$, $\gamma = 10$ and $\varepsilon = 0.5$.

$$U = V = 0,\ \frac{\partial \varphi^*}{\partial n} = -\frac{D_T^*}{D_B^*}\cdot\frac{1}{N_{BT}}\cdot\frac{1}{1+\delta\theta}\frac{\partial \theta}{\partial n},\ \theta_{(m,s)} = 1, \tag{34}$$

On the right cold wavy surface: $A(1-\cos(2N\pi X)),\ 0 \le Y \le 1$

$$U = V = 0,\ \frac{\partial \varphi^*}{\partial n} = -\frac{D_T^*}{D_B^*}\cdot\frac{1}{N_{BT}}\cdot\frac{1}{1+\delta\theta}\frac{\partial \theta}{\partial n},\ \theta_{hnf} = 0, \tag{35}$$

On the adiabatic bottom horizontal surface:

$$U = V = 0,\ \frac{\partial \varphi^*}{\partial n} = 0,\ \frac{\partial \theta_{(hnf,m,s)}}{\partial n} = 0. \tag{36}$$

The dimensionless boundary positions through the interface permeable surface between the hybrid nanofluid and the porous layer and by considering the similar dynamic viscosity ($\mu_{hnf} = \mu_m$) in both layers. Therefore, the interface dimensionless boundary conditions are formulated in the following form (Zargartalebi et al., 2016):

$$\theta_{hnf}|_{Y=D^+} = \theta_m|_{Y=D^-}, \tag{37}$$

$$\left.\frac{\partial \theta_{hnf}}{\partial Y}\right|_{Y=D^+} = \left.\frac{k_{eff}}{k_{nf}}\frac{\partial \theta_m}{\partial Y}\right|_{Y=D^-}, \tag{38}$$

$$U_{hnf}|_{Y=D^+} = U_m|_{Y=D^-}, \tag{39}$$

$$V_{hnf}|_{Y=D^+} = V_m|_{Y=D^-}, \tag{40}$$

$$\varphi^*|_{Y=D^+} = \varphi^*|_{Y=D^-}, \tag{41}$$

$$\frac{\partial \varphi^*}{\partial n}|_{Y=D^+} = \frac{\partial \varphi^*}{\partial n}|_{Y=D^-}, \tag{42}$$

where D performs the hybrid nanofluid layer's thickness and the subscripts + and − are indicated the corresponding quantities that estimated while approaching the interface of the porous and hybrid nanofluid layers, respectively. $Ra = \frac{g\beta_f(T_h-T_c)L^3}{\nu_f\alpha_f}$, $\mathrm{Pr} = \frac{\nu_f}{\alpha_f}$ and $\alpha_f = \frac{k_f}{(\rho C_p)_f}$ are Rayleigh number, Prandtl number and thermal diffusivity of the base liquid (water).

The local Nusselt numbers (Nu_{nf} and Nu_s) at the wavy vertical (left) surface for hybrid nanofluid and solid phases, respectively, as follows:

$$Nu_{nf} = -\frac{k_{eff}}{k_f}\left(\frac{\partial \theta_{hnf}}{\partial \mathrm{n}}\right)_{\mathrm{n}}. \tag{43}$$

$$Nu_s = -\frac{k_s}{k_f}\left(\frac{\partial \theta_s}{\partial \mathrm{n}}\right)_{\mathrm{n}}, \tag{44}$$

here n determines the entire length of the curved heat source.

Lastly, the average Nusselt numbers at the wavy vertical surface within the hybrid nanofluid and the solid phases are given by the following equations:

$$\overline{Nu}_{nf} = \int_0^{\mathrm{n}} Nu_{nf}\,\mathrm{dn}, \tag{45}$$

$$\overline{Nu}_s = \int_0^{\mathrm{n}} Nu_s\,\mathrm{dn}. \tag{46}$$

3. Numerical method and validation

The governing dimensionless equations Eqs. (24)–(32) subject to the boundary conditions (33)–(42) do solve by the Galerkin weighted residual finite element technique. The computational region does discretize toward small triangular portions.

These small triangular Lagrange components with various forms are applied to each flow variable within the computational region. Residuals for each conservation equation exist accomplished through substituting the approximations within the governing equations. The Newton–Raphson iteration algorithm is adopted for clarifying the nonlinear expressions into the momentum equations. The convergence from the current numerical solution does consider, while the corresponding error toward each of the variables does fill the resulting convergence criteria:

$$\left|\frac{\Gamma^{i+1}-\Gamma^i}{\Gamma^{i+1}}\right| \le \eta,$$

where i represents the iteration number and η is the convergence criterion. In this study, the convergence criterion was set at $\eta = 10^{-6}$ (see Fig. 2).

Concerning the validation of current data, the existing outcomes examine among earlier published experimental outcomes that achieved by Beckermann et al. (1988) for natural convection within a square cavity having fluid and porous layers, as shown in Fig. 3. Besides, the existing outcomes are associated with previously published numerical outcomes received by Khanafer et al. (2009) concerning the situation of natural convection heat transfer into a wavy non-Darcian porous cavity, as exhibited within Fig. 4. The numerical outcomes concerning the current code produce a high degree of reliability according to these achievements.

4. Results and discussion

Outcomes represented through streamlines, isotherms of nanofluid phase, isotherms of solid phase, and nanoparticle concentration are

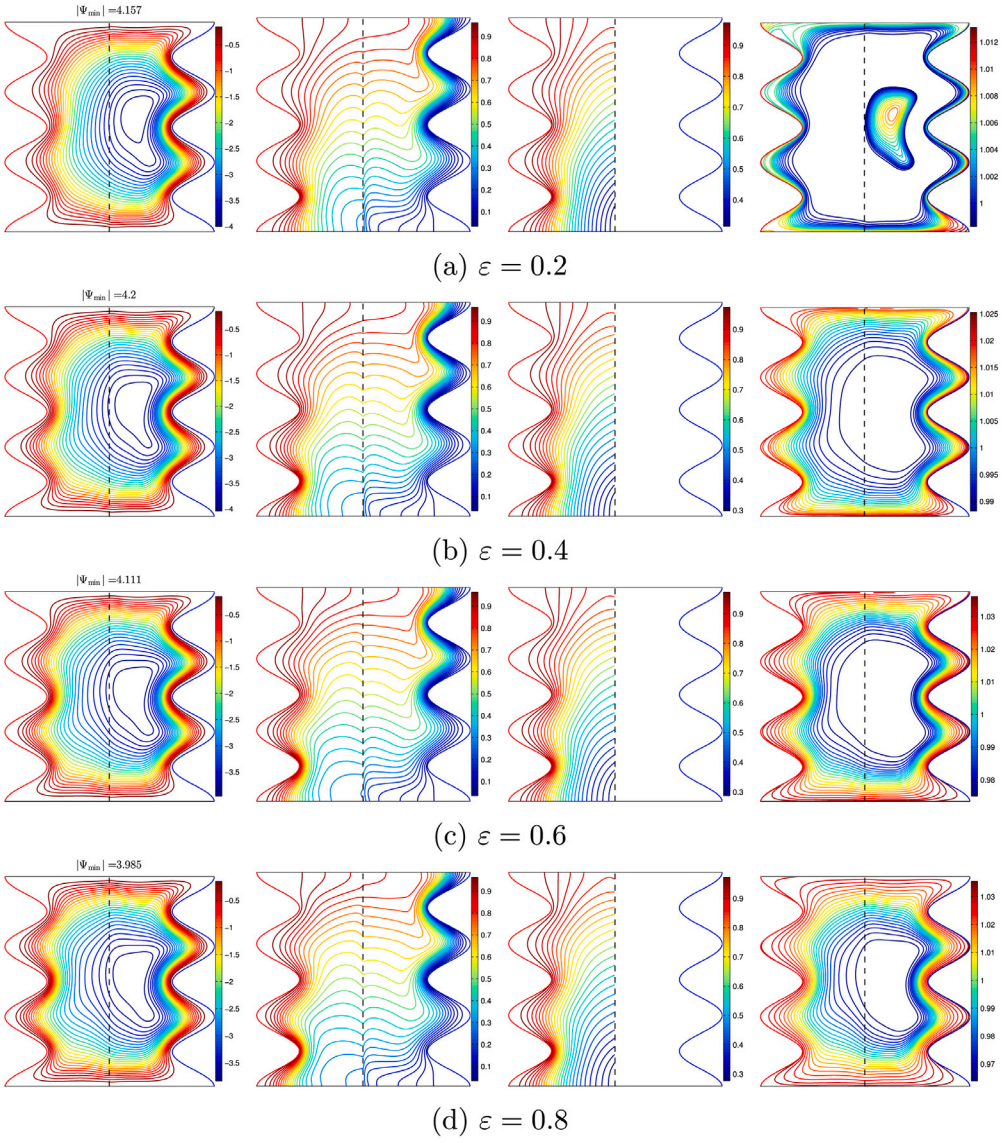

Fig. 11. Streamlines, isotherms of nanofluid phase, isotherms of solid phase and nanoparticle distribution with various porosity of the medium (ε); hybrid nanofluid, $Da = 10^{-3}$, $\phi = 0.02$, $\gamma = 10$ and $A = 0.1$.

Table 1
Thermo-physical properties of water, Cu nanoparticles, Al_2O_3 nanoparticles and glass balls at $T = 310$K (Bergman and F.P., 2011).

Physical properties	Fluid phase (water)	Cu	Al_2O_3	Glass balls
C_p (J/kgK)	4178	385	765	840
$\mu \times 10^6$ (kg/ms)	695	–	–	–
ρ (kg/m^3)	993	8933	3970	3100
k (Wm^{-1}K^{-1})	0.628	400	40	1.05
$\beta \times 10^5$ (1/K)	36.2	1.67	0.85	–
d_p (nm)	0.385	29	33	–

examined into this segment. We modified the following four parameters; Darcy number ($10^{-6} \leq Da \leq 10^{-2}$), nanoparticle volume fraction ($0 \leq \phi \leq 0.04$), modified conductivity ratio ($0.1 \leq \gamma \leq 1000$), amplitude ($0 \leq A \leq 0.2$) and the porosity of the medium ($0.2 \leq \varepsilon \leq 0.8$). The values of Rayleigh number, number of undulations, inter-phase heat transfer coefficient and Prandtl number are fixed at $Ra = 10^6$, $N = 3$, $H = 10$ and Pr = 4.623, respectively. Table 1 displays the thermos-physical properties of the base fluid (water), solid Cu and Al_2O_3 phases at $T = 310$K.

Fig. 5 depicts the streamlines, isotherms for fluid and solid phases, and the nanoparticle distribution within the cavity for different values of the Darcy number (Da). The cavity is heated from the left, so the heated fluid in that region goes upwards and is replaced by cold fluid coming from the right side, resulting in a flow recirculation cell moving in the clockwise direction. It can be seen that for $Da = 10^{-5}$, the flow is mostly taking place in the region of free nanofluid, as limited streamlines are seen in the porous medium region. As Da increases above that value, the flow takes over in the whole cavity, and the intensity of circulation intensifies, as evidenced by the value of the absolute stream function. Indeed, Da is an indicator of the medium's permeability and the ease at which the fluid can flow inside it, which explains the intensification of the flow at higher Da. The nanofluid isotherms are directed vertically near the walls where conductive heat transfer is dominant. The isotherms become horizontal in the middle of the fluid circulation cell, indicating an intensification of the convective heat transfer where the nanofluid is flowing. So this remains limited to the free circulation zone for $Da = 10^{-5}$. This behavior can be observed in the discontinuities that appear in the fluid streamlines for low Da at the interface between the porous medium and the free region. The

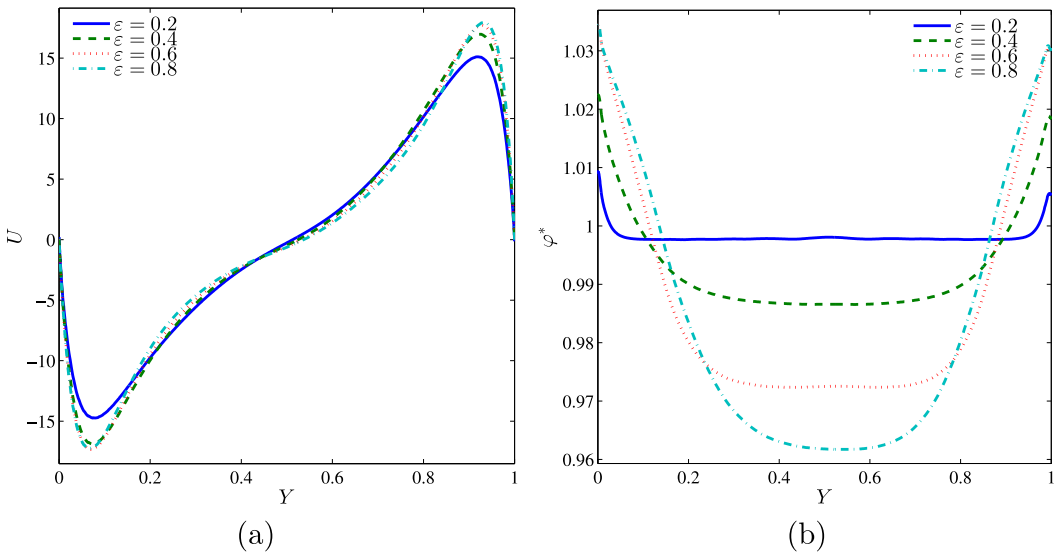

Fig. 12. Local velocity (a) and local normalized solid volume fraction (b) with the vertical line (interface) (Y) for $X = 0.5$ for different ε; hybrid nanofluid, $Da = 10^{-3}$, $\phi = 0.02$, $\gamma = 10$ and $A = 0.1$.

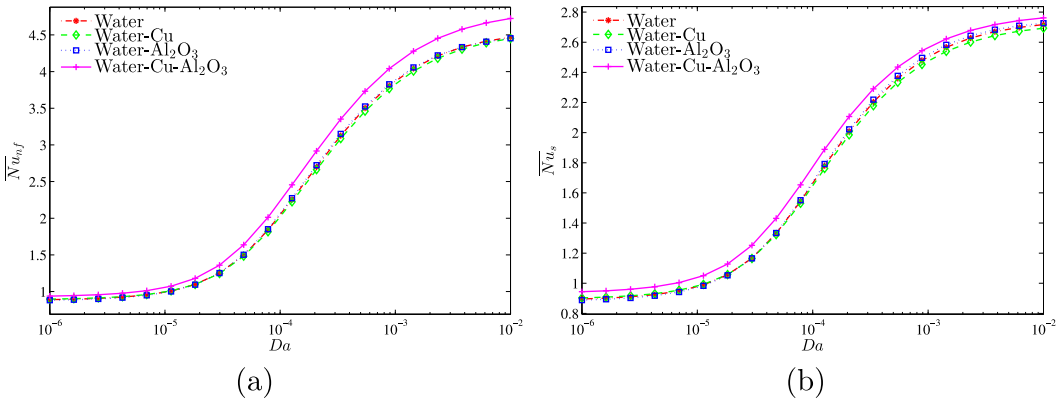

Fig. 13. Variations of (a) average Nusselt number of nanofluid phase and (b) average Nusselt number of solid phase with Da for different for various types of nanoparticles at $\phi = 0.02$, $\gamma = 10$, $A = 0.1$ and $\varepsilon = 0.5$.

solid streamlines show a low sensibility to the variation of Da as their shape shows a slight variation when Da is increased.

On the other hand, the isotherms of the solid and nanofluid phases are very similar for low Da, indicating a thermal equilibrium between the two phases. This thermal equilibrium vanishes when Da is increased, as the increase of convective heat transfer in the fluid tends to raise the temperature difference between the nanofluid and the porous layer. The nanoparticles are concentrated near the walls in all the cases, while lower concentrations are seen in the middle of the cavity. The nanoparticles' concentration is greater near the cold right wall compared to the left hot wall due to the thermophoretic force that tends to move the particles in a direction as opposed to the thermal gradient, i.e., from the high-temperature zones to the lower temperature zones.

To better illustrate the distributions of the flow velocity and the nanoparticle distribution, Fig. 6 shows the variations of the local velocity U and the local normalized solid volume fraction φ^* along with the vertical interface for various values of Da. It is shown that the velocity over the interface is close to zero for $Da = 10^{-5}$, as in that case, the flow is limited to the free zone, and the interface acts as a sidewall due to the very low permeability of the porous medium. When Da is raised, the velocity magnitude increases due to the reduced resistance of the porous medium. The velocity is positive in the bottom half and negative in the bottom one, indicating the flow's clockwise direction. As for the nanoparticle volume fraction, it is clear that it is greater than 1 near the upper and lower walls, while it is less than 1 in the middle region, confirming the higher concentration tendency near the wall. Nonetheless, the nanoparticles present a more uniform distribution for $Da = 10^{-5}$, when the flow is limited in the zone to the right of the interface. For $Da = 10^{-2}$, when the porous material has a negligible effect on the flow due to the nanofluid's enhanced convective effects.

The streamlines, the isothermal contours, and the nanoparticle distribution contours are plotted in Fig. 7 for different values of the conductivity ratio γ. The streamlines show similar patterns in all the cases. The main effect of γ appears in the isotherms contours. It is clear that increasing γ tends to assimilate the isotherms of the fluid phase to those of the solid phase, indicating that the thermal equilibrium can be applied in that case. In fact, as can be seen from Eq. (29), the temperature difference between the solid matrix and the nanofluid is greater when γ is reduced. Changing γ shows a slight effect on the nanoparticle concentration near the walls, while the nanoparticles' distribution is more uniform for the highest value of γ. This is due to the thermal non-equilibrium observed for lower γ, and the amplification of the thermophoretic force at the interface between the solid and liquid phases in that case. These observations are confirmed in Fig. 8, which illustrates the variations of U and φ^* along with the vertical interface for different values of γ. The magnitude of the velocity shows a higher amplitude when γ is reduced, indicating flow intensification. At the

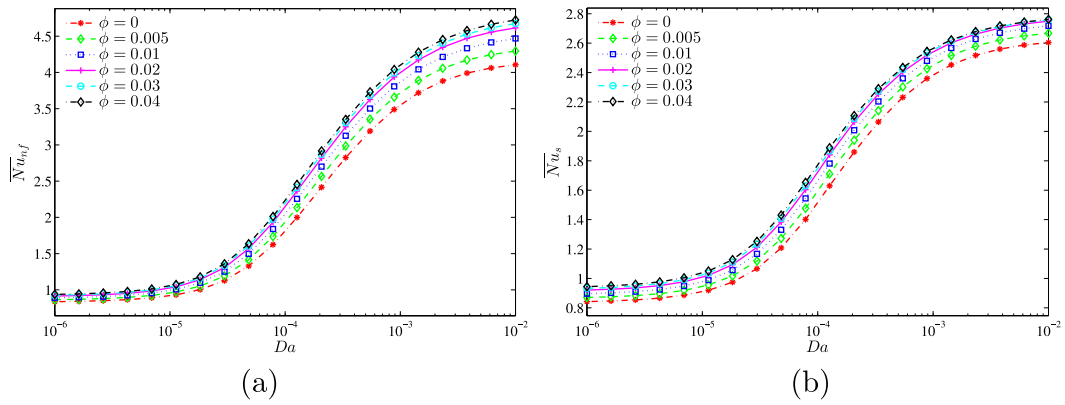

Fig. 14. Variations of (a) average Nusselt number of nanofluid phase and (b) average Nusselt number of solid phase with Da for different ϕ at hybrid nanofluid, $\gamma = 10$, $A = 0.1$ and $\varepsilon = 0.5$.

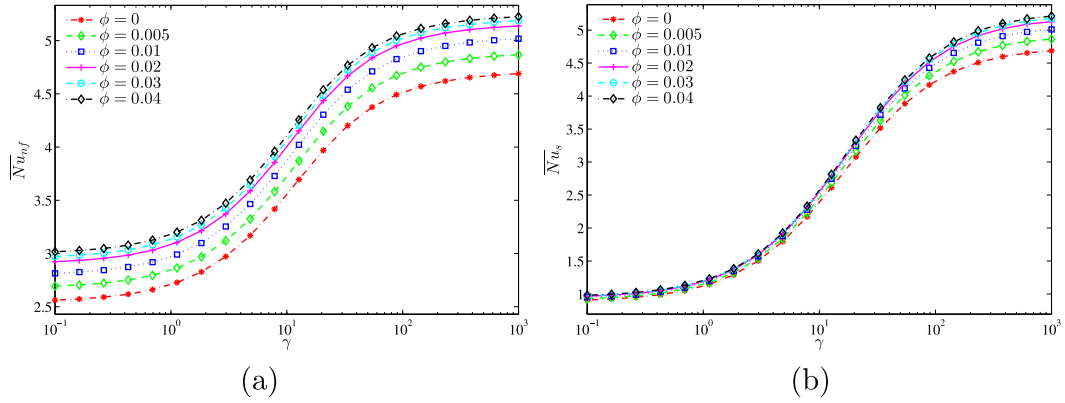

Fig. 15. Variations of (a) average Nusselt number of nanofluid phase and (b) average Nusselt number of solid phase with γ for different ϕ at hybrid nanofluid, $Da = 10^{-3}$, $A = 0.1$ and $\varepsilon = 0.5$.

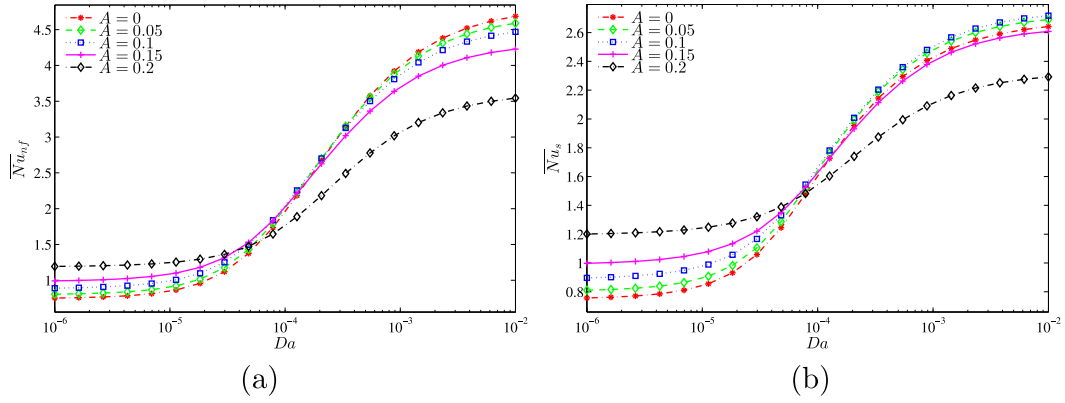

Fig. 16. Variations of (a) average Nusselt number of nanofluid phase and (b) average Nusselt number of solid phase with Da for different A at hybrid nanofluid, $\phi = 0.02$, $\gamma = 10$ and $\varepsilon = 0.5$.

same time, the volume fraction shows a higher concentration near the upper and lower walls, with a more uniform distribution when γ is increased.

The effect of the wall undulation amplitude A on the flow and isothermal patterns and on the nanoparticle distribution is shown in Fig. 9. The value $A = 0$ represents a square cavity with straight walls. The main effect of the wall undulation is the disturbance of the flow patterns by creating a larger flow boundary layer near the walls. This results in a stagnant flow in the wavy wall crests and localized high velocities near the wall troughs. When A is increased to 0.2, two recirculation cells appear in the cavity and are localized in the central region. The isotherms follow the variation of the streamlines and shift toward the center when A is increased. For $A = 0$ and $A = 0.1$, the isotherms are horizontal in the middle of the cavity, pointing out a dominant convective heat transfer. The convective effects are diminished for $A = 0.2$ when the flow is squeezed into the central region.

Moreover, in the last case, the isotherms of the fluid and solid phases are closer to each other, indicating an intensification of the thermal non-equilibrium when A is reduced. Following these observations, the concentration of the nanoparticle near the walls is more pronounced for lower A. The variations of U and φ^* along with the vertical interface,

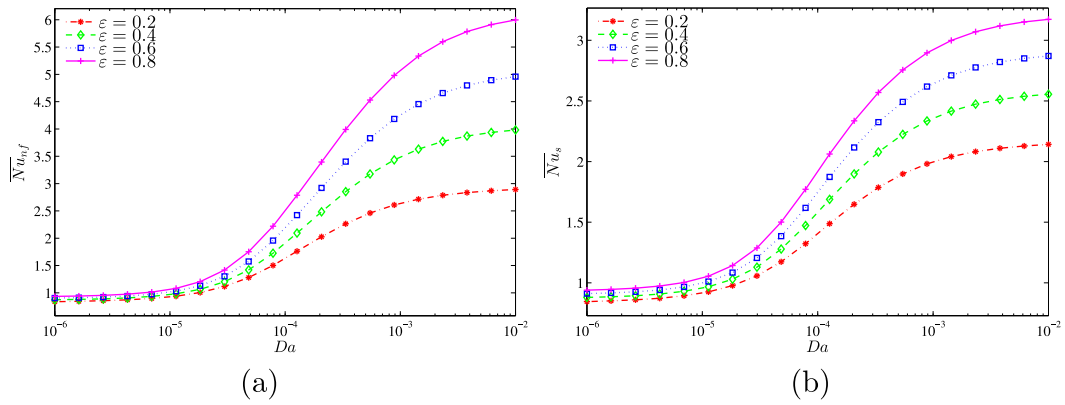

Fig. 17. Variations of (a) average Nusselt number of nanofluid phase and (b) average Nusselt number of solid phase with Da for different ε at hybrid nanofluid, $\phi = 0.02$, $\gamma = 10$ and $A = 0.1$.

plotted in Fig. 10 for various values of A, confirm the localized increase in velocity when A is increased above 0.1 due to the wall undulation. Moreover, it can be seen that the distribution of the nanoparticles along the interface is more uniform for higher A and disturbed by the high undulation amplitude.

Fig. 11 shows the streamlines, isotherms, and contours of nanoparticle distribution concerning different values of the medium porosity ε. The parameter ε has a similar effect to the parameter Da discussed in Fig. 5, in the sense that it also captures the thermal resistance of the porous medium. Nonetheless, it also indicates the contribution of the solid matrix within the porous medium to heat transfer. In fact, an increase in ε indicates a lower volume portion of the solid part, and therefore, more freedom for the nanofluid to flow. This results in a higher velocity amplitude for higher ε, as exhibited by Fig. 12, despite presenting similar flow patterns. On the other hand, when ε is raised, less thermal interaction among nanofluid and solid phases from the porous material, which results in a higher shift between the fluid and solid isotherms. As for the nanoparticles, despite remaining further concentrated adjacent to the surfaces, a less uniform pattern remains existing for higher ε, as observed in Fig. 12, which is due to the rise of the thermophoretic effects on the interface within the solid layer and the nanofluid at the interface resulting from the temperature difference.

The variations of the average Nusselt numbers for the fluid phase $\overline{Nu}_{nf}$ and for the solid phase $\overline{Nu}_{s}$ as functions of Da are plotted in Fig. 13 for different nanofluid types. Both $\overline{Nu}_{nf}$ and $\overline{Nu}_{s}$ increase with the rise of Da. This increase is slow for Da lower than 10^{-5}; then the slope is sharp before starting to stabilize after $Da = 10^{-3}$. $\overline{Nu}_{nf}$ and $\overline{Nu}_{s}$ increase respectively by around 4.5 and 2.7 times when Da is elevated from 10^{-5} to 10^{-2}. For very low Da, the flow resistance provided by the porous slows down the fluid and hinders heat transfer. Once the fluid starts to move with more ease at higher Da, the heat transfer intensifies, as indicated by the rise of the Nusselt numbers. Regarding the nanoparticle type, a slight increase in the values of Nusselt number is observed for the Water–Cu–Al_2O_3 nanofluid compared to the others, indicating a better heat transfer when a hybrid nanofluid is used.

The variations of $\overline{Nu}_{nf}$ and $\overline{Nu}_{s}$ as functions of Da are plotted in Fig. 14 for various values of the nanoparticle concentration ϕ. It is clear that both $\overline{Nu}_{nf}$ and $\overline{Nu}_{s}$ increase for higher ϕ. The lowest rates of the Nusselt number continue to perform within the case of a pure fluid ($\phi = 0$). Such observation illustrates the importance of adding nanoparticles to the enhancement of the thermal conductivity of the nanofluid. This trend of variation is more apparent as Da grows, which intensifies the flow circulation. However, increase in Nusselt number is not substantial, as only a 17% rise in $\overline{Nu}_{nf}$ is observed when ϕ is increased from 0 to 0.04 for $Da = 10^{-2}$.

Fig. 15 illustrates the impact of φ on the variations of $\overline{Nu}_{nf}$ and $\overline{Nu}_{s}$ as functions of γ. The trend of variation γ with is similar to the one observed in the two previous graphs with Da. For low γ, typically less than 1, $\overline{Nu}_{nf}$ and $\overline{Nu}_{s}$ increase with a low slope with γ, then an abrupt rise in $\overline{Nu}_{nf}$ and $\overline{Nu}_{s}$ is present when δ is between 1 and 100 due to the improvement of the thermal conductivity of the fluid, before stabilizing for γ greater than 100. The effect of ϕ on the variations of the two Nusselt numbers is less pronounced for $\overline{Nu}_{s}$ compared to $\overline{Nu}_{nf}$, as the nanoparticles mainly affect heat transfer in the nanofluid. Nonetheless, similar to the observation of Fig. 14, Both Nusselt numbers increase when ϕ is raised.

Fig. 16 shows the variations of $\overline{Nu}_{nf}$ and $\overline{Nu}_{s}$ as functions of Da for various values of A. For low Da, approximatively less than 10^{-4}, the two Nusselt numbers increase for higher values of A and are maximum for $A = 0.2$. However, when Da is raised beyond that value, the opposite trend occurs and both $\overline{Nu}_{nf}$ and $\overline{Nu}_{s}$ have their minimal values obtained for $A = 0.2$. The effect of the amplitude A on the average Nusselt numbers depends on the value of Da. In fact, for low Da, when the flow circulation is hindered by the increased solid volume in the porous medium, the rise of the undulation amplitude provides better mixing in the fluid and better thermal transfer with the solid matrix. When Da is increased, the convective effects are enhanced due to the intensified flow circulation. In that case, raising the amplitude of the undulations reduces the flow intensity due to the greater flow boundary layer and the stagnant fluid zones that may occur in the wavy wall crests.

For large values of Darcy number, Fig. 16(b) shows that the Nusselt number increases by the increase of amplitude when A in the range of 0 to 0.1. However, further increase of amplitude significantly decreases the average Nusselt number of the solid phase. When the amplitude is small, there is a uniform temperature gradient along hot surface and the increase of the amplitude reduces the distance between the hot and cold regions and boosts the temperature gradient and consequently average $\overline{Nu}_{s}$. However, a further increase of the amplitude results in building regions between undulations with high temperatures but low temperature gradients, which tend to change the trend of the results and decrease $\overline{Nu}_{s}$.

The effect of ε on the variations of $\overline{Nu}_{nf}$ and $\overline{Nu}_{s}$ as functions of Da is illustrated in Fig. 17. For low Da, the effect of ε is negligible, as the flow resistance is great regardless of the porosity. On the other hand, for Da greater than 10^{-4}, raising ε leads to a considerable increase in the Nusselt numbers, due to the enhanced flow circulation and resulting heat transfer. $\overline{Nu}_{nf}$ gets 6 times higher when ε is raised from 0.2 to 0.8 for $Da = 10^{-2}$.

5. Conclusions

The problem of natural convection steady flow and the heat transfer concerning hybrid nanofluids inside a complex cavity with wavy

hot and cold sidewalls is considered. The hybrid nanofluid was modeled using the non-homogeneous procedure, and the distribution of nanoparticles in the enclosure was analyzed using concentration contours. The concentration of composite nanoparticles was low at the enclosure's central regions and high next to the walls. The significant conclusions regarding the existing research will be summarized as follows:

1. Raising the Darcy number Da intensifies the flow circulation due to the increased permeability. This results in more important convective effects and enhanced heat transfer. 4.5 and 2.7 times respective increase is observed in $\overline{Nu}_{nf}$ and $\overline{Nu}_{s}$ when Da is varied from 10^{-5} to 10^{-2}. The thermal equilibrium within the solid and liquid in the porous medium remains more evident for the lower Da. The nanoparticles are concentrated near the walls, with more important concentrations adjacent to the right wavy cold surface, due to the thermophoretic force that moves the particle from hot zones toward the cold ones.
2. Increasing the ratio of thermal conductivity γ within the nanofluid and the solid matrix improves heat transfer due to the nanofluid's improved thermal conductivity. Moreover, raising γ improves the thermal equilibrium among the solid and liquid phases and results in a more uniform distribution of the nanoparticles and the interface within the porous and free liquid zones.
3. A slight improvement in heat transfer is obtained when the nanoparticle concentration is increased. $\overline{Nu}_{nf}$ raises by 17% when ϕ is increased from 0 to 0.04 for $Da = 10^{-2}$. Moreover, this improvement is better when a hybrid water–Cu–Al_2O_3 is used compared to other nanofluids.
4. The effect of the amplitude A of the wall undulations depends on the value of Da. For low Da, using a cavity with a greater value of A enhances heat transfer, while the opposite is observed for higher values of Da.

The summary of these results can be helpful for the design of thermal systems based on nanofluids and porous media, to optimize the design parameters for a better performance and lower cost. The focus should be on the selection of the nanoparticles of the nanofluid, as well as on the material of the porous medium and its permeability. As observed, increasing the thermal conductivity ratio between the nanofluid and the porous medium, and increasing the permeability in the enclosure are more efficient in enhancing heat transfer compared to the use of wavy walls instead of straight ones. In addition, using Cu-Al_2O_3 based hybrid nanofluids was found more performant. However, topics such as the cost associated with the different technical solutions can be subject of future research.

CRediT authorship contribution statement

Ammar I. Alsabery: Conceptualization, Methodology, Software, Validation, Preparation. **Ahmad Hajjar:** Visualization, Investigation, Methodology, Writing – original draft. **Zehba A.S. Raizah:** Visualization, Investigation, Methodology, Writing – original draft. **Mohammad Ghalambaz:** Visualization, Investigation, Methodology, , Writing – original draft. **Ishak Hashim:** Methodology, Writing – review & editing. **Ali J. Chamkha:** Investigation, Editing.

Declaration of competing interest

The authors declare that they have no known competing financial interests or personal relationships that could have appeared to influence the work reported in this paper.

Acknowledgments

We are grateful for the financial support received from the Universiti Kebangsaan Malaysia (UKM) under the research grant GP-2020-K006388. Also, the authors would like to extend their appreciations to the Deanship of Scientific Research at King Khalid University, Abha, Saudi Arabia, for funding this work through the Research Group Project under grant number R.G.P2/144/42.

References

Ahmed, S.E., Rashed, Z.Z., 2019. MHD natural convection in a heat generating porous medium-filled wavy enclosures using Buongiorno's nanofluid model. Case Stud. Therm. Eng. 14, 100430.

Almuhtady, A., Alhazmi, M., Al-Kouz, W., Raizah, Z.A.S., Ahmed, S.E., 2021. Entropy generation and MHD convection within an inclined trapezoidal heated by triangular fin and filled by a variable porous media. Appl. Sci. 11 (4), 1951.

Alomar, O.R., Basher, N.M., Yousif, A.A., 2020. Analysis of effects of thermal non-equilibrium and non-Darcy flow on natural convection in a square porous enclosure provided with a heated l shape plate. Int. J. Mech. Sci. 181, 105704.

Alsabery, A.I., Armaghani, T., Chamkha, A.J., Hashim, I., 2020. Two-phase nanofluid model and magnetic field effects on mixed convection in a lid-driven cavity containing heated triangular wall. Alex. Eng. J. 59 (1), 129–148.

Alsabery, A.I., Ismael, M.A., Chamkha, A.J., Hashim, I., 2019b. Effects of two-phase nanofluid model on MHD mixed convection in a lid-driven cavity in the presence of conductive inner block and corner heater. J. Thermal Anal. Calorimetry 135 (1), 729–750.

Alsabery, A.I., Mohebbi, R., Chamkha, A.J., Hashim, I., 2019a. Effect of local thermal non-equilibrium model on natural convection in a nanofluid-filled wavy-walled porous cavity containing inner solid cylinder. Chem. Eng. Sci. 201, 247–263.

Alsabery, A.I., Tayebi, T., Chamkha, A.J., Hashim, I., 2018. Effect of rotating solid cylinder on entropy generation and convective heat transfer in a wavy porous cavity heated from below. Int. Commun. Heat Mass Transfer 95, 197–209.

Aly, A.M., Raizah, Z.A.S., 2020. Incompressible smoothed particle hydrodynamics simulation of natural convection in a nanofluid-filled complex wavy porous cavity with inner solid particles. Physica A 537, 122623.

Ambreen, T., Saleem, A., Park, C.W., 2020. Analysis of hydro-thermal and entropy generation characteristics of nanofluid in an aluminium foam heat sink by employing Darcy-Forchheimer–Brinkman model coupled with multiphase Eulerian model. Appl. Therm. Eng. 173, 115231.

Ashorynejad, H.R., Shahriari, A., 2018. MHD natural convection of hybrid nanofluid in an open wavy cavity. Results Phys. 9, 440–455.

Baytas, A.C., Pop, I., 2002. Free convection in a square porous cavity using a thermal nonequilibrium model. Int. J. Therm. Sci. 41 (9), 861–870.

Beckermann, C., Viskanta, R., Ramadhyani, S., 1988. Natural convection in vertical enclosures containing simultaneously fluid and porous layers. J. Fluid Mech. 186, 257–284.

Bergman, T.L., F.P., Incropera, 2011. Introduction To Heat Transfer, sixth ed. Wiley, New York.

Bondareva, N.S., Sheremet, M.A., Oztop, H.F., Abu-Hamdeh, N., 2016. Heatline visualization of MHD natural convection in an inclined wavy open porous cavity filled with a nanofluid with a local heater. Int. J. Heat Mass Transfer 99, 872–881.

Borah, A., Pati, S., 2021. Influence of non-uniform asymmetric heating on conjugate heat transfer in a rectangular minichannel using nanofluid by two-phase Eulerian-Lagrangian method. Powder Technol. 381, 164–180.

Bozorg, M.V., Siavashi, M., 2019. Two-phase mixed convection heat transfer and entropy generation analysis of a non-Newtonian nanofluid inside a cavity with internal rotating heater and cooler. Int. J. Mech. Sci. 151, 842–857.

Celli, M., Impiombato, A.N., Barletta, A., 2020. Buoyancy-driven convection in a horizontal porous layer saturated by a power-law fluid: The effect of an open boundary. Int. J. Therm. Sci. 152, 106302.

Chen, Y.Y., Li, B.W., Zhang, J.K., 2016. Spectral collocation method for natural convection in a square porous cavity with local thermal equilibrium and non-equilibrium models. Int. J. Heat Mass Transfer 96, 84–96.

Chen, Y.Y., Li, B.W., Zhang, J.K., Qian, Z.D., 2018. Influences of radiative characteristics on free convection in a saturated porous cavity under thermal non-equilibrium condition. Int. Commun. Heat Mass Transfer 95, 80–91.

Cho, C.C., 2020. Effects of porous medium and wavy surface on heat transfer and entropy generation of Cu–water nanofluid natural convection in square cavity containing partially-heated surface. Int. Commun. Heat Mass Transfer 119, 104925.

Corcione, M., 2011. Empirical correlating equations for predicting the effective thermal conductivity and dynamic viscosity of nanofluids. Energy Convers. Manage. 52 (1), 789–793.

Das, D., Biswal, P., Roy, M., Basak, T., 2016. Role of the importance of 'Forchheimer term' for visualization of natural convection in porous enclosures of various shapes. Int. J. Heat Mass Transfer 97, 1044–1068.

Elshehabey, H.M., Raizah, Z., Öztop, H.F., Ahmed, S.E., 2020. MHD natural convective flow of Fe_3O_4-H_2O ferrofluids in an inclined partial open complex-wavy-walls ringed enclosures using non-linear Boussinesq approximation. Int. J. Mech. Sci. 170, 105352.

Filahi, I., Hasnaoui, M., Amahmid, A., Bourich, M., 2021. Double-diffusive natural convection study in a shallow horizontal porous layer filled with a binary fluid and submitted to destabilized conditions in the presence of soret effect. Materials Today: Proceedings http://dx.doi.org/10.1016/j.matpr.2021.01.685.

Ghalambaz, M., Tahmasebi, A., Chamkha, A.J., Wen, D., 2019. Conjugate local thermal non-equilibrium heat transfer in a cavity filled with a porous medium: Analysis of the element location. Int. J. Heat Mass Transfer 138, 941–960.

Ghasemi, K., Siavashi, M., 2017. Lattice Boltzmann numerical simulation and entropy generation analysis of natural convection of nanofluid in a porous cavity with different linear temperature distributions on side walls. J. Molecular Liquids 233, 415–430.

Haider, F., Hayat, T., Alsaedi, A., 2021. Flow of hybrid nanofluid through Darcy-Forchheimer porous space with variable characteristics. Alex. Eng. J. 60 (3), 3047–3056.

Hussain, S., Ismael, M.A., Chamkha, A.J., 2020. Impinging jet into an open trapezoidal cavity partially filled with a porous layer. Int. Commun. Heat Mass Transfer 118, 104870.

Khanafer, K., Al-Azmi, B., Marafie, A., Pop, I., 2009. Non-Darcian effects on natural convection heat transfer in a wavy porous enclosure. Int. J. Heat Mass Transfer 52 (7–8), 1887–1896.

Khoei, A.R., Sichani, A.S., Hosseini, N., 2020. Modeling of reactive acid transport in fractured porous media with the extended–FEM based on Darcy-Brinkman-Forchheimer framework. Comput. Geotech. 128, 103778.

Li, Z., Barnoon, P., Toghraie, D., Dehkordi, R.B., Afr, M., 2019. Mixed convection of non-Newtonian nanofluid in an H-shaped cavity with cooler and heater cylinders filled by a porous material: Two phase approach. Adv. Powder Technol. 30 (11), 2666–2685.

Mehryan, S.A.M., Ghalambaz, M., Chamkha, A.J., Izadi, M., 2020. Numerical study on natural convection of Ag–MgO hybrid/water nanofluid inside a porous enclosure: A local thermal non-equilibrium model. Powder Technol. 367, 443–455.

Mikhailenko, S.A., Sheremet, M.A., 2020. Impacts of rotation and local element of variable heat generation on convective heat transfer in a partially porous cavity using local thermal non-equilibrium model. Int. J. Therm. Sci. 155, 106427.

Miroshnichenko, I.V., Sheremet, M.A., Oztop, H.F., Abu-Hamdeh, N., 2018. Natural convection of alumina-water nanofluid in an open cavity having multiple porous layers. Int. J. Heat Mass Transfer 125, 648–657.

Misirlioglu, A., Baytas, A.C., Pop, I., 2005. Free convection in a wavy cavity filled with a porous medium. Int. J. Heat Mass Transfer 48 (9), 1840–1850.

Molana, M., Dogonchi, A.S., Armaghani, T., Chamkha, A.J., Ganji, D.D., Tlili, I., 2020. Investigation of hydrothermal behavior of Fe_3O_4-H_2O nanofluid natural convection in a novel shape of porous cavity subjected to magnetic field dependent (MFD) viscosity. J. Energy Storage 30, 101395.

Mutschler, D., Mojtabi, A., 2020. Theoretical and numerical analysis of soret-driven convection in a horizontal porous layer saturated by an n-component mixture: Application to ternary hydrocarbon mixture tetralin, isobutyl benzene, n-dodecane with mass fractions 0.8-0.1-0.1. Int. J. Heat Mass Transfer 162, 120339.

Nayak, M.K., Shaw, S., Khan, M.I., Pandey, V.S., Nazeer, M., 2020. Flow and thermal analysis on Darcy-Forchheimer flow of copper–water nanofluid due to a rotating disk: A static and dynamic approach. J. Mater. Res. Technol. 9 (4), 7387–7408.

Nguyen, M.T., Aly, A.M., Lee, S.W., 2015. Natural convection in a non-Darcy porous cavity filled with Cu–water nanofluid using the characteristic-based split procedure in finite-element method. Numer. Heat Transfer Part A: Appl. 67 (2), 224–247.

Nield, D.A., Bejan, A., et al., 2006. Convection in Porous Media, vol. 3. Springer.

Oğlakkaya, F.S., Bozkaya, C., 2018. Unsteady MHD mixed convection flow in a lid-driven cavity with a heated wavy wall. Int. J. Mech. Sci. 148, 231–245.

Parveen, R., Mahapatra, T.R., 2019. Numerical simulation of MHD double diffusive natural convection and entropy generation in a wavy enclosure filled with nanofluid with discrete heating. Heliyon 5 (9), e02496.

Raizah, Z., Aly, A.M., 2021. Double-diffusive convection of a rotating circular cylinder in a porous cavity suspended by nano-encapsulated phase change materials. Case Stud. Therm. Eng. 24, 100864.

Rashed, Z., Alhazmi, M., Ahmed, S.E., 2021. Non-homogenous nanofluid model for 3D convective flow in enclosures filled with hydrodynamically and thermally heterogeneous porous media. Alex. Eng. J. 60 (3), 3119–3132.

Rashed, Z.Z., Mansour, M.A., Attia, M.A., Ahmed, S.E., 2020. Numerical study of radiative impacts on a magneto-convective flow confined an inclined two-sided wavy enclosure using hybrid nanofluid. Phys. Scr. 96 (2), 025216.

Revnic, C., Groşan, T., Sheremet, M., Pop, I., 2020. Numerical simulation of MHD natural convection flow in a wavy cavity filled by a hybrid Cu-Al_2O_3-water nanofluid with discrete heating. Appl. Math. Mech. 41 (9), 1345–1358.

Sadeghi, M.S., Tayebi, T., Dogonchi, A.S., Nayak, M.K., Waqas, M., 2021. Analysis of thermal behavior of magnetic buoyancy-driven flow in ferrofluid–filled wavy enclosure furnished with two circular cylinders. Int. Commun. Heat Mass Transfer 120, 104951.

Selimefendigil, F., Öztop, H.F., 2020. Effects of local curvature and magnetic field on forced convection in a layered partly porous channel with area expansion. Int. J. Mech. Sci. 179, 105696.

Shenoy, A., Sheremet, M., I., Pop, 2016. Convective Flow and Heat Transfer from Wavy Surfaces: Viscous Fluids, Porous Media, and Nanofluids. CRC press, Taylor & Francis Group, Boca Raton.

Sheremet, M.A., Cimpean, D.S., Pop, I., 2017a. Free convection in a partially heated wavy porous cavity filled with a nanofluid under the effects of Brownian diffusion and thermophoresis. Appl. Therm. Eng. 113, 413–418.

Sheremet, M.A., Revnic, C., Pop, I., 2017b. Free convection in a porous wavy cavity filled with a nanofluid using Buongiorno's mathematical model with thermal dispersion effect. Appl. Math. Comput. 299, 1–15.

Sivasankaran, S., Do, Y., Sankar, M., 2011. Effect of discrete heating on natural convection in a rectangular porous enclosure. Transp. Porous Media 86 (1), 261–281.

Wang, L., Huang, C., Hu, J., Shi, B., Chai, Z., 2021. Effects of temperature-dependent viscosity on natural convection in a porous cavity with a circular cylinder under local thermal non-equilibrium condition. Int. J. Therm. Sci. 159, 106570.

Wang, C.Y., Mobedi, M., Kuwahara, F., 2019. Analysis of local thermal non-equilibrium condition for unsteady heat transfer in porous media with closed cells: Sparrow number. Int. J. Mech. Sci. 157, 13–24.

Zargartalebi, H., Ghalambaz, M., Noghrehabadi, A., Chamkha, A.J., 2016. Natural convection of a nanofluid in an enclosure with an inclined local thermal non-equilibrium porous fin considering Buongiorno's model. Numer. Heat Transfer Part A: Appl. 70 (4), 432–445.

Zhang, X., Su, G., Lin, J., Liu, A., Wang, C., Zhuang, Y., 2021. Three-dimensional numerical investigation on melting performance of phase change material composited with copper foam in local thermal non-equilibrium containing an internal heater. Int. J. Heat Mass Transfer 170, 121021.